https://doi.org/10.17221/70/2019-CJGPB

Comparative metabolomics and transcriptomics of pistils, stamens and pistilloid stamens widen key knowledge of pistil and stamen development in wheat

*Yan Yu[1,3], Zheng Song Peng[2], Ji Peng Qu[2], Zhen Yong Chen[1], Shu Hong Wei[1], Ming Li Liao[1], Li Zhang[3], Zai Jun Yang[1]**

[1]*Key Laboratory of Southwest China Wildlife Resources Conservation (Ministry of Education), College of Life Science, China West Normal University, Nanchong, Sichuan, P.R. China*
[2]*School of Agricultural Science, Xichang University, Xichang, Sichuan, P.R. China*
[3]*College of Sciences, Sichuan Agricultural University, Ya'an, Sichuan, P.R. China*
**Corresponding author: yangzaijun1@126.com*

Citation: Yu Y., Peng Z.S., Qu J.P., Chen Z.Y., Wei S.H., Liao M.L., Zhang L., Yang Z.J. (2020): Comparative metabolomics and transcriptomics of pistils, stamens and pistilloid stamens widen key knowledge of pistil and stamen development in wheat. Czech J. Genet. Plant Breed., 56: 24–33.

Abstract: To examine the role of metabolites in wheat stamen and pistil development, metabolomic analyses of pistilloid stamens (PS), pistils (P), and stamens (S) from a novel wheat mutant homologous transformation sterility-1 (HTS-1) and controls from their sib-line CSTP were conducted using base gas chromatography-mass spectrometry (GC-MS) and liquid chromatography-mass spectrometry (LC-MS). Then, the metabolomic data were integrated with previously published transcriptomic data and analysed. In total, 141 annotated metabolites were determined from P, PS and S tissues by comparison with reference standards. A total of 90, 93 and 18 different metabolites were identified in S *vs.* PS, S *vs.* P and P *vs.* PS, respectively. Among the different metabolites, 80 may be associated with stamen and pistil growth. Using integration evaluations of both the previous transcriptome data and the 80 various metabolites, we found two perturbed pathways that significantly affect flower development in plants, namely, the phenylpropanoid biosynthesis and cysteine and methionine metabolism. The ethylene synthesis pathway, one key branch of the cysteine and methionine metabolic pathways, could have a pivotal role in pistillody growth involving HTS-1. We found two key enzyme genes in the ethylene synthesis pathway (the SAM synthase gene and the ACC synthase gene) that have higher expression levels in stamens than in pistilloid stamens or pistils. We speculate, that the decrease in ethylene content during stamen development leads to pistillody traits in HTS-1. This study helps elucidate the molecular mechanisms underlying stamen and pistil growth in wheat.

Keywords: metabolome; pistillody; transcriptome; *Triticum aestivum* L.; wheat

Wheat (*Triticum aestivum* L.) is a major global food source, and approximately 11.02% of the global wheat cultivation area (22.16 million ha per year) is situated within China (FAO 2017). However, the recent estimates of wheat yield in China indicated 5481 kg/ha, which is considerably less than the yields of rice or corn (FAO 2017). Therefore, a primary goal of wheat breeding is to develop traits that increase yield. The utilization of heterosis is an effective way to improve wheat yield. Despite the previous

Supported by the National Natural Science Foundation of China (Grant No. 31760425), National General Cultivation Project of China West Normal University (Grant No. 17C043), and the Innovation Team Project of China West Normal University (Grant No. CXTD2018-6).

https://doi.org/10.17221/70/2019-CJGPB

advancements in growing wheat hybrids, these improvements have not been utilised due to the absence of an appropriate sterile male line. The wheat mutant homologous transformation sterility-1 (HTS-1) was first detected in the offspring of a cross between a three-pistil (TP) mutant and Chinese Spring (CS) (Peng *et al*. 2013). HTS-1 and Chinese Spring three pistils (CSTP) are considered sib-lines that exhibit the three-pistil trait, which has been associated with the *Pis1* gene. Nevertheless, the HTS-1 phenotype is mainly distinguished by pistillody, incomplete or full stamen changes into pistils or similar structures (Sommer *et al*. 1990; Goto & Meyerowitz 1994; Zhang *et al*. 2007). More severe HTS-1 mutants develop 6 pistils and no stamens and very low seed-setting rates (average: 15.3%) despite innate pollination states (Peng *et al*. 2013). HTS-1 is unlike the additional pistillody mutants, including alloplasmic lines of wheat cultivars Norin 26 (N26) and (cr)-CSdt7BS, which are due to nuclear-cytoplasm interactions (Murai & Tsunewaki 1993; Murai *et al*. 2002), as well as the MADS-box gene *TaAGL2* (Yamada *et al*. 2009). Nevertheless, pistillody in HTS-1 is induced by 2 recessive genes (Peng *et al*. 2013). Wheat flowers are very stable, and a few mutants have been reported to date. Earlier investigations involving wheat floret mutants only provide limited information on floral organ identity determination. Thus, evaluation of HTS-1 in relation to pistil and stamen growth in wheat is essential, and this mutant also has the potential to be a sterile male line for use in wheat hybrid breeding.

Compared to genomic and transcriptomic studies in wheat (Yang *et al*. 2017; Zimin *et al*. 2017), wheat metabolomic studies have received relatively limited attention. Secondary metabolites often perform remarkable physiological functions (Wang *et al*. 2018). The integrated analysis of transcriptomes and metabolites provides a novel way to explore new genes and to study gene regulation and stress resistance. Via a comprehensive transcriptome and metabolite strategy, Bielecka *et al*. (2014) identified novel genes that were associated with glucosinolate metabolism in response to sulphur deficiency, whereas Tohge *et al*. (2005) characterised a new flavonoid biosynthesis pathway in transgenic MYB-overexpressing *Arabidops*is plants. Kaplan *et al*. (2007) previously described sequential alterations involving gene expression and metabolite profiles throughout cold acclimation.

In the study reported here, we analysed the integrated metabolome and transcriptome data derived from pistilloid stamens (PS) and pistils (P) via HTS-1 plants and via stamens (S) taken from the control CSTP sib-lines. Our results may provide an understanding of pistil and stamen growth in wheat.

MATERIAL AND METHODS

Plant material. HTS-1 is a new wheat sterile-male mutant that was chosen during the development of CSTP (Peng *et al*. 2013). CSTP is a near-isogenic line of Chinese Spring (CS) and carries the *Pis1* gene that comes from the TP mutant (Yang *et al*. 2011). Thus, CSTP and HTS-1 are sib-lines that have nearly identical phenotypes, with the exception of pistillody. HTS-1 and CSTP were maintained in our laboratory and were grown in a field in China West Normal University, Nanchong, China. PS and P in HTS-1 and S in the CSTP at the heading stage were chosen for gas chromatography-mass spectrometry (GC-MS) and liquid chromatography-mass spectrometry (LC-MS) evaluation. The PS, P, and S were separately gathered 6 times, producing 6 biological replicates.

GC-MS analysis. A GC-MS evaluation was conducted with a modification of the strategy previously outlined by Lisec *et al*. (2006). We transferred 100 mg of the plant samples into 5 ml centrifuge tubes, added five steel balls and then placed them into liquid nitrogen for 5 min. The tubes were placed in a high flux organization grinding apparatus at 70 Hz for 1 min. We added 400 µl of methanol (precooled to –20°C), vortexed the tubes for 30 s and then added 60 µl of ribitol (0.2 mg per ml dissolved in methanol) as an internal quantitative standard and then vortexed for 30 s. The tubes were subjected to ultrasonication at room temperature for 30 min, to which 750 µl of chloroform (precooled to –20°C) and 1400 µl of deionised water (dH_2O) (4°C) were added, followed by vortexing for 60 s. The tubes were centrifuged at 14 000 rpm at 4°C for 10 min, and then, 1 ml of the supernatant was collected into a centrifuge tube and vacuum-dried. Approximately 60 µl of 15 mg/ml methoxyamine pyridine solution was added, vortexed for 30 s, and then allowed to react for 120 min at 37°C. Then, 60 µl of BSTFA reagent (containing 1% TMCS) was added into the mixture and allowed to react for 90 min at 37°C. The tubes were centrifuged at 12 000 rpm at 4°C for 10 min. The supernatant was extracted and split into two aliquots; one was utilised for metabolite measurements, whereas the other was stored at –20°C.

A 1-µl aliquot was used for GC-MS (Agilent 7890A GC/5975C MS, Agilent, USA) evaluation. An HP-5MS

https://doi.org/10.17221/70/2019-CJGPB

capillary column (30 m × 250 µm × 0.25 µm, Agilent, USA) and quadrupole detector were employed. The following conditions were used: injection temperature, 280°C; interface, 150°C; and ion source, 230°C. The temperature ramp programme had an initial temperature of 60°C for 2 min, a 10°C/min rate up to 300°C, and then held at 300°C for 5 min. Mass spectrometry was performed using the full-scan strategy, ranging from 35 m/z to 750 m/z.

LC-MS analysis. LC-MS analysis was conducted with an alteration of the strategy previously outlined by De Vos *et al.* (Lisec *et al.* 2006). Plant samples were crushed as in section GC-MS analysis, and then, we added 1000 µl of methanol (precooled to –20°C) and vortexed them for 30 s. The tubes were placed into an ultrasonicator at room temperature for 30 min, after which we added 750 µl of chloroform (precooled to –20°C) and 800 µl deionised water (dH_2O) (4°C) and vortexed the tubes for 60 s. The tubes were centrifuged for 10 min at 12 000 rpm 4°C, and then, 1 ml of the supernatant was moved into a different centrifuge tube. The specimens were dried via vacuum concentration. For LC-MS detection, the samples were dissolved in 250 µl of a methanol aqueous solution (1 : 1, 4°C) and filtered through a 0.22-µm membrane.

Chromatographic separation was achieved in an Acquity UPLC system outfitted with an ACQUITY UPLC® HSS T3 (150 × 2.1 mm, 1.8 µm, Waters, USA) column set at 40°C. The autosampler temperature was 4°C. Gradient elution of the analytes was conducted using 0.1% formic acid in water (A) as well as 0.1% formic acid in acetonitrile (B), with a flow rate of 0.25 ml/min. A 3-µl aliquot of each specimen was injected following equilibration. We used an increasing linear gradient of solvent B (v/v) as described: 0~1 min, 2% B; 1~9.5 min, 2~50% B; 9.5~14 min, 50%~98% B; 14~15 min, 98% B; 15~15.5 min, 98~2% B; 15.5~17 min; 2% B. The ESI-MS^n experiments were conducted on a Thermo LTQ-Orbitrap XL mass spectrometer (Thermo, USA) using respective spray voltages of 4.8 kV and –4.5 kV as positive and negative modes. Sheath and auxiliary gases were set to 40 and 15 arbitrary units, respectively. The capillary temperature was 325°C. Capillary and tube voltages were 35 V and 50 V in the respective positive and negative modes of –15 V and –50 V. The Orbitrap analyser was employed for a full scan across a range of m/z 50–1000 and at 60 000 mass resolution. Data-dependent acquisition (DDA) MS/MS experiments were conducted using a CID scan. The normalised collision energy was 30 eV. We implemented dynamic exclusion using a repeat count of 2 and a 15-c exclusion duration.

Statistical analysis. GC/MSD ChemStation Software (Agilent) was employed for data collection and for GC total ion chromatogram and metabolite mass spectral generation. The original GC-MS data were converted into files in netCDF format (Smith *et al.* 2006) and subsequently preprocessed, including the identification, filtration, and alignment of peaks by XCMS software (www.bioconductor.org). Finally, a data matrix of information, including mass-to-charge ratios (m/z), retention times, and peak intensities, was obtained. Identification of metabolites was performed using the AMIDS system (Automated Mass Spectral Deconvolution and Identification System) by searching the National Institute of Standards and Technology library (http://srdata.nist.gov/gateway/) and the Wiley Chemical Structure Library (Oberacher *et al.* 2013). Area normalisation was employed for quantitative analysis. LC-MS data were identified by an automated identification script using the METLIN and MONA databases, and the total peak area normalisation was utilised for quantitative analysis. We also use 30 standard chemical to confirm the qualitative of the identified chemical (Table S2 and S3 in Electronic Supplementary Material (ESM) with yellow colour). Principal component analysis (PCA) models were produced with Simca-P (Ver. 13.0, 2009) software. The metabolic profiling data of the three samples were analysed using Student's *t* test to determine the metabolites with significant differences among samples. A fold change (FC) value was calculated for every annotated metabolite to quantify the difference between two samples. |FC| > 1.5 or |lg2FC| > 0.58 and *P*-value < 0.05 were chosen for further analysis (Heischmann *et al.* 2016). We previously identified 206 common differentially expressed genes (DEGs) in PS *vs.* P and P *vs.* S by transcriptomic analysis (Yang *et al.* 2015). In addition, enriched Kyoto Encyclopedia of Genes and Genomes (KEGG) pathways associated with those 206 DEGs and metabolite levels were identified using InCroMAP (Eichner *et al.* 2014).

Real-time PCR. Total RNA was isolated from P, PS and S. cDNA was synthesised with a PrimeScript Perfect real-time RT reagent kit (TaKaRa, China) following the manufacturer's protocol. The primers for the SAM synthase, ACC synthase and ACC oxidase genes were designed with Beacon Designer to amplify short fragments (Table S1 in ESM). Via a

https://doi.org/10.17221/70/2019-CJGPB

Bio-Rad CFX96 real-time PCR platform, real-time assays were conducted with SYBR Green (TaKaRa, China). All specimens were analysed in triplicate, and the fold change in the number of RNA transcripts was quantified with the $2^{-\Delta\Delta ct}$ method (Livak & Schmittgen 2001) with the wheat housekeeping genes ubiquitin (DQ086482) and actin (AB181911) acting as internal controls (Hama *et al.* 2004; Yamada *et al.* 2009).

RESULTS

Determination of metabolites using GC-MS and LC-MS. The metabolic profiling of the P, PS and S was performed with GC-MS and LC-MS. Total ion chromatograms (TICs) and base peak chromatograms (BPCs) (Figure S1 in ESM) revealed variable chromatographic characteristics among organs. The retention time was stable and reproducible, suggesting the efficacy and reliability of the metabolomics evaluation. In all, 141 annotated metabolites were identified from P, PS and S in contrast with reference standards, of which 68 metabolites were separated by GC-MS and 73 by LC-MS (Table S2 and S3 in ESM). These metabolites may be further classified into nine types of chemicals, which include organic acids, amino acids, sugars, fatty acids, nucleotides, phosphoric acids, polyols, amines and others. Of the metabolite groups, the chemical classes of organic acids and amino acids accounted for the largest proportion, accounting for 32% and 23% of all identified metabolites, respectively. Relatively few sugars (7%), fatty acids (6%), nucleotides (5%), phosphoric acids (5%), polyols (4%) or amines (1%) were identified (Figure 1).

Principal component analysis (PCA) of metabolites. To examine the general clustering patterns between the different organs, PCA with the unsupervised projection strategy was applied to the metabolite profiling acquired from the P, PS and S. Figure 2 demonstrated that three principal components (PCs) were obtained, which accounted for 65.7% of the total variance. The P and PS were differentiated clearly from S along PC1. We also observed that the PS and P were separated, but the separation was not obvious (Figure 2).

Different metabolites (DMs) among PS, P, and S. To determine the metabolite differences among PS, P and S, metabolites with a fold change (FC) > 1.5 or an lg2FC > 0.58 and *P*-value < 0.05 were chosen for further analysis (Heischmann *et al.* 2016).

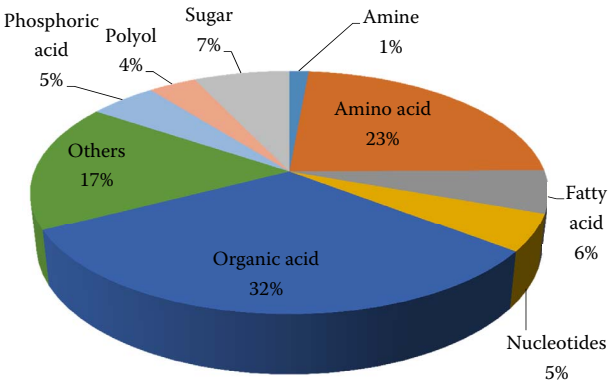

Figure 1. The 141 metabolites were classified into 9 different chemical classes, including organic acids, amino acids, sugars, fatty acids, nucleotides, phosphoric acids, polyols, amines and others

The number of DMs in S *vs.* PS was 90, including 53 upregulated metabolites and 37 downregulated metabolites (Figure 3A, Table S4 in ESM). There were 93 DMs in S *vs.* P, including 50 upregulated metabolites and 43 downregulated metabolites (Figure 3A, Table S5 in ESM). However, there were only 18 DMs in P *vs.* PS, including 14 upregulated metabolites and 4 downregulated metabolites (Figure 3A, Table S6 in ESM). This tendency suggests that PS and P have nearly identical metabolome profiles. Among the DMs, 80 DMs were shared between S *vs.* PS and S *vs.* P, which included 47 up- as well as 33 downregulated metabolites (Figure 3B, Table 1). These 80 DMs might play crucial roles in stamen and pistil growth in wheat. Among the 80 DMs, there were 40 primary metabolites, such as amino acids, fatty acids,

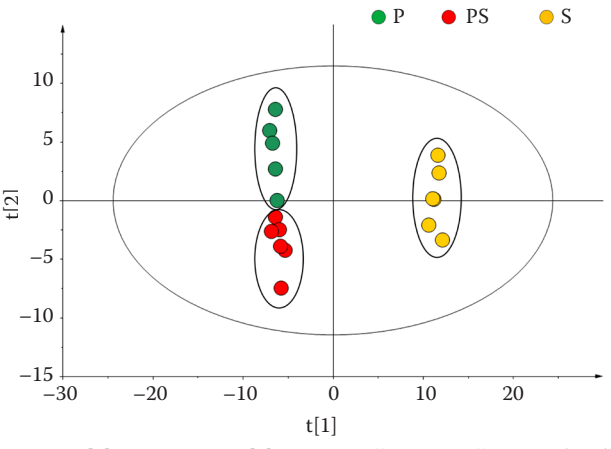

Figure 2. Principle component analysis (PCA) of metabolites in pistils (P), pistilloid stamens (PS) and stamens (S)

https://doi.org/10.17221/70/2019-CJGPB

Table 1. The 80 different metabolites that shared between in stamens (S) *vs.* pistilloid stamens (PS) and stamens *vs.* pistils (P)

Metabolite	Retention time (min)	log2FC(S *vs.* PS)	log2FC(S *vs.* P)
(5-Hydroxyindol-3-yl) acetic acid	11.50	9.83	9.70
Glutathione disulfide	4.43	9.23	9.03
2-(2-Carboxyethyl)-4-methyl-5-propylfuran-3-carboxylic acid	11.79	8.23	8.25
(–)-Fusicoplagin A	11.64	6.94	8.03
5-S-Methyl-5-thioadenosine	5.36	5.58	5.21
Glucaric acid	18.26	5.32	5.89
Alanine	6.86	4.60	3.69
Aspartic acid	1.51	4.59	4.80
3,5-Cyclic GMP	4.52	4.58	4.89
3-Hydroxybenzoic acid	9.21	4.48	3.83
7H-Xanthine	3.95	4.47	4.33
5-Methylthioadenosine	24.44	4.44	4.59
2,3-Dihydroxybutanedioic acid	13.77	4.09	4.21
2-Aminoadipic acid	14.97	4.02	3.93
(2S)-2-Isopropyl-3-oxosuccinic acid	4.19	3.95	3.57
Methionine	12.68	3.70	3.68
Serine	10.67	3.24	2.78
Adenine	1.73	3.13	3.52
Homoserine	11.83	2.97	2.70
D-Gluconic acid	1.57	1.76	2.66
Isoleucine	9.71	2.97	2.46
Glutaminyl-valine	4.97	2.69	2.08
2,4-Dihydroxybutanoic acid	11.35	2.57	2.40
Beta-alanopine	6.24	2.54	1.56
4-Hydroxybenzoic acid	13.94	2.38	2.09
4-Hydroxyproline	12.81	2.32	2.29
Guanine	4.11	2.27	2.14
Threonine	11.03	2.02	1.60
Lactamide	1.48	1.97	1.94
Pantothenate	6.83	1.93	1.54
Glutamine	1.51	1.86	1.61
Guanosine	4.11	1.66	1.43
Tryptophan	5.57	1.62	1.29
9-(*Z*)-Octadecenoic acid	19.79	1.59	0.75
Arginine	1.42	1.55	1.67
Beta-alanine	11.50	1.55	1.43
Monomethylphosphate	8.05	1.32	1.41
Itaconic acid	4.47	1.32	1.75
Uridine	3.47	1.31	0.96
Ribose	14.69	0.73	1.15
Phenylalanine	4.77	1.19	0.90
Inosine	5.08	1.15	1.79
Glycine	9.90	0.99	1.04
Uracil	10.34	0.81	0.81

https://doi.org/10.17221/70/2019-CJGPB

Table 1 to be continued

Metabolite	Retention time (min)	log2FC(S *vs.* PS)	log2FC(S *vs.* P)
Heptanoic acid	7.91	0.79	0.83
Threonic acid	13.29	0.76	0.87
4-Aminobutyric acid	12.81	0.73	0.68
Citric acid	16.18	–0.62	–0.82
Pipecolic acid	10.68	–0.65	–1.25
Shikimic acid	16.02	–0.91	–0.74
Maltitol	24.68	–1.03	–0.74
Threitol	12.65	–1.10	–1.18
Di-(ethylhexyl) phthalate	14.68	–1.10	–0.82
Sorbitol	17.48	–1.24	–1.13
trans-3-Coumaric acid	3.58	–1.42	–1.57
Sorbitol-6-phosphate	21.19	–1.49	–1.67
Isocitric acid	2.70	–1.51	–1.77
4-Oxopentanoic acid	15.52	–1.64	–1.23
4-Hydroxy-crotonic acid	15.52	–1.66	–1.22
gamma-glutamylphenylalanine	5.97	–1.70	–1.90
Frucose-6-phosphate	20.93	–2.08	–2.25
Myo-inositol-1-phosphate	21.81	–2.79	–2.80
Proline	1.66	–2.90	–2.89
Adenosine	4.03	–3.28	–3.54
9-Hydroxy pelargonic acid	8.67	–3.40	–4.40
Glucose-6-phosphate	21.04	–3.41	–3.47
Succinyladenosine	4.83	–3.56	–3.95
N-Acetylvanilalanine	7.76	–3.56	–3.95
Myo-inositol	18.94	–3.58	–3.84
Glutamic acid	13.88	–3.76	–4.03
6-P-Gluconic acid	21.44	–3.81	–3.35
Maltose	24.36	–3.82	–3.55
N-Acetyl-L-phenylalanine	7.75	–3.82	–4.09
Alpha-kamlolenic acid	13.82	–4.03	–4.92
Sucrose	23.59	–4.17	–4.10
8R,11S-DiHODE	13.82	–4.48	–5.66
9,10-12,13-Diepoxyoctadecanoate	12.45	–4.78	–5.25
Avenoleic acid	13.38	–5.72	–6.38
2-Ketoglutaric acid	13.37	–7.43	–7.46
Lysine	3.85	–8.24	–8.56

nucleotides and sugars. There were 40 secondary metabolites, such as organic acids, phosphoric acid and polyol, among others.

Integration analysis of metabolomics with transcriptomics. We previously identified 206 common DEGs in PS *vs.* P and in P *vs.* S and speculated that the 206 genes were correlated to wheat stamen and pistil development (Yang *et al.* 2015). Here, we identified a relationship between the 206 DEGs and the 80 DMs. The list of metabolites, correlated genes and KEGG pathways is provided in Table S7. We found two pathways that significantly affect flower development in plants: phenylpropanoid biosynthesis and cysteine and methionine metabolism (Table S7 in ESM).

https://doi.org/10.17221/70/2019-CJGPB

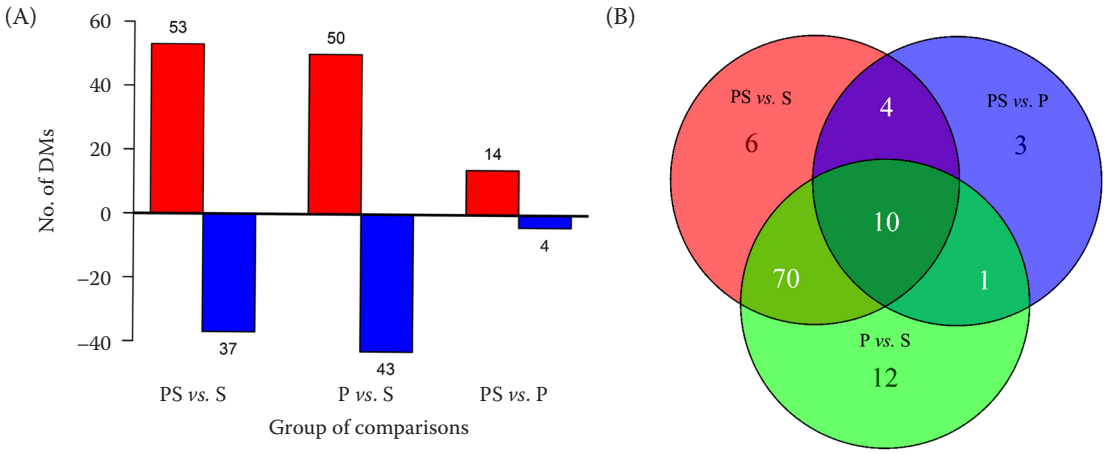

Figuer 3. Different metabolites (DMs) among pistils (P), pistilloid stamens (PS) and stamens (S): (A) histogram showing DMs among pistils, pistilloid stamens and stamens (red means up metabolites, blue means down metabolites), (B) Veen diagram showing DMs among pistils, pistilloid stamens and stamens

In the phenylpropanoid biosynthesis pathway, the metabolite phenylalanine was upregulated in S; the log2 FC (S *vs.* PS) and log2 FC (S *vs.* P) were 1.19 and 0.90, respectively. There were six DEGs, including beta-glucosidase 22, cinnamyl alcohol dehydrogenase 7, peroxidase 1, peroxidase 44, peroxidase 2, and serine carboxypeptidase-like 18. Among these DEGs (except for cinnamyl alcohol dehydrogenase 7), the gene expression levels were upregulated in S (https://www.genome.jp/dbget-bin/www_bget?ko00940, Figure S2 in ESM, Table 1). There were six DMs (alanine, aspartic acid, serine, methio-

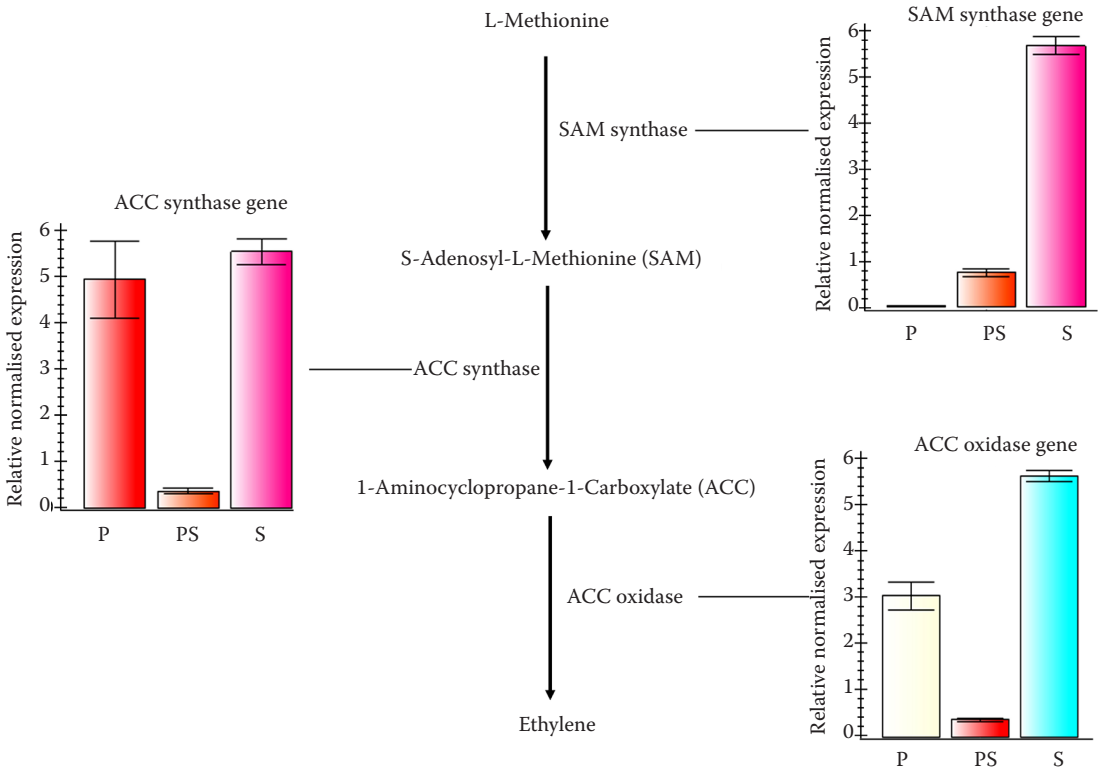

Figure 4. The expression pattern of key genes in ethylene synthesis pathway
P – pistils; PS – pistilloid stamens; S – stamens; the transcript levels are shown as relative values and the columns represent the means ± SEM of three replicate

https://doi.org/10.17221/70/2019-CJGPB

nine, 5-S-methyl-5-thioadenosine and homoserine) in the cysteine and methionine metabolism pathways. These DMs were upregulated in S and downregulated in P and PS (Table 1). This metabolic pathway also includes the ethylene biosynthesis pathway, and the speed-limiting enzyme ACC oxidase gene in ethylene synthesis had upregulated expression in S and downregulated expression in P and PS (https://www.genome.jp/dbget-bin/www_bget?ko00270, Figure S3 and Table S7 in ESM).

Expression analysis of primary genes in the ethylene synthesis pathway. Many studies have shown that ethylene affects flower development (Carbonell-Bejerano *et al*. 2011; Tao *et al*. 2018). In this evaluation, we integrated the analysis of metabolomics with transcriptomics and found that the expression of the gene for the speed-limiting enzyme ACC oxidase in the ethylene synthesis pathway was upregulated in S and downregulated in P and PS. To further confirm the relationship between ethylene and the pistilloid structures in wheat, the expression patterns of key genes in the ethylene synthesis pathway (involving the SAM synthase, ACC synthase and ACC oxidase genes) were studied by real-time PCR in P, PS and S. As shown in Figure 4, the SAM synthase gene has a higher expression level in S (approximately 60-fold and 8-fold higher than P and PS, respectively). The ACC synthase gene had a similar expression pattern in P and S but showed very low expression in PS, only a quarter of that found in S (Figure 4). The ACC oxidase gene was upregulated in S, which was approximately 13-fold greater than that observed in PS. This was followed by elevated ACC oxidase expression in P, which was approximately 7.5-fold greater than PS. The lowest level of expression was observed in PS (Figure 4).

DISCUSSION

This study sought to identify small molecules and genes associated with pistil and stamen development in wheat. Two complementary GC and LC-MS approaches were used to distinguish metabolites between S and PS, S and P, and P and PS. The metabolome data were then integrated with previously published transcriptomics data for the comprehensive dissection of alterations during pistil and stamen development in wheat.

PCA was used to assess the changes in the metabolome among the P, PS and S samples (Figure 2). As expected, the metabolite profiles of P, PS and S reflected tissue specificity. However, the metabolic profiles of P and PS were similar, with only a small number of metabolites exhibiting significant differences (Figure 3A, Table S6 in ESM). This finding agrees with the published transcriptomic results (Yang *et al*. 2015). Our analysis identified 80 DMs that were shared between S and P and S and PS (Table 1). Thus, these 80 DMs likely play important roles in pistil and stamen growth since the P and PS have nearly identical morphological structures and metabolome profiles. Approximately half of these DMs are primary metabolites; previous studies have shown that the primary metabolites play a key role in cell proliferation and differentiation (Cuadrosinostroza *et al*. 2016; Yu *et al*. 2019). However, whether the primary metabolites have a direct relationship with the development of wheat flowers has not been reported.

We used integration to analyse both the 206 DEGs and 80 DMs and found two flower development pathways that were significantly affected. These were the phenylpropanoid biosynthesis and cysteine and methionine metabolism. The phenylpropanoid biosynthesis pathway generates a wide range of structurally variable molecules, such as hydroxycinnamic acids and flavonoids, including flavonols, anthocyanins, dihydrochalcones, and their glycoside derivatives (Dare *et al*. 2017). Phenylpropanoids are considered 'secondary metabolites', possibly playing a less critical role during plant growth and development. Previous studies have established the role of these compounds in providing structural support, UV tolerance, and reactions to pathogens (Ferreyra *et al*. 2012). There is also growing evidence that these metabolites modulate plant growth and development (Peer & Murphy 2007). In particular, flavonoids, which are synthesised through the phenylpropanoid pathway, play important roles in plant sterility (Mo *et al*. 1992). In this study, we found that phenylalanine, an important precursor in the flavonoid biosynthesis pathway, was downregulated in PS (log2FC (S *vs.* PS) = 1.19). Therefore, we speculated that flavonoids may be related to the sterility in HTS-1.

The ethylene synthesis pathway is a key branch of the cysteine and methionine metabolism pathways. In the ethylene synthesis pathway, SAM synthase from L-methionine catalyses the formation of S-adenosyl-L-methionine (SAM), and 1-aminocyclopropane-1-carboxylate (ACC) is the immediate precursor of ethylene and is synthesized from SAM by ACC synthase. ACC oxidase catalyses the last step of ethylene synthesis, utilizing ACC as a substrate and producing carbon dioxide and cyanide (Wang *et al*. 2002). Ethylene is a plant hormone that influences various developmental processes, such as seed germination,

https://doi.org/10.17221/70/2019-CJGPB

flowering, ripening of fruits, senescence and abscission (Liu *et al*. 2016). In unisexual flowering plants, such as cucumbers and lemons, ethylene has a key role in sex determination and has long been utilized in the induction of female flowers in horticultural generation (Rudich 1969; Tsao 1988; Yin & Quinn 1995). In cucumbers, exogenous ethylene or the ethylene predecessor ACC has been employed to promote female flower formation in monoecious plants (Yamasaki *et al*. 2003), whereas interference of ethylene synthesis or signalling triggers the production of male flowers in gynoecious plants (Takahashi & Jaffe 1983). However, the role of ethylene in the development of bisexual flowers has not been documented. In the current evaluation, we found that two key enzyme genes from the ethylene synthesis pathway (the SAM and ACC synthase genes) have higher expression levels in S (Figure 4). This finding may mean that stamen development in wheat requires more ethylene relative to pistils. Therefore, we hypothesize that the decrease in ethylene content during stamen development leads to pistillody traits in HTS-1. The role of ethylene in the flower growth of wheat appears to be the opposite of that seen in the unisexual flowering plants. Our prior evaluations have also revealed that ethylene metabolism is connected to the pistillody trait (Yang *et al*. 2018; Sun *et al*. 2019). However, it is not clear how ethylene regulates stamen and pistil development in wheat, and additional work is needed.

In conclusion, to evaluate the impact of metabolites on the development of stamens and pistils in wheat, a metabolomics analysis of PS, P, and S was conducted based on GC-MS and LC-MS. Then, the metabolome data were integrated with previously published transcriptomics data and analysed. Our results revealed 80 DMs and two pathways that might be putatively correlated with stamen and pistil development. In particular, the ethylene synthesis pathway may play a major role in pistillody in HTS-1. This study provides a novel understanding of the molecular mechanisms essential to wheat stamen and pistil growth.

References

Bielecka M., Watanabe M., Morcuende R., Scheible W.R., Hawkesford M.J., Hesse H. (2014): Transcriptome and metabolome analysis of plant sulfate starvation and resupply provides novel information on transcriptional regulation of metabolism associated with sulfur, nitrogen and phosphorus nutritional responses in *Arabidopsis*. Frontiers in Plant Science, 5: 805.

Carbonell-Bejerano P.,Urbez C., Granell A., Carbonell J., Perez-Amador M.A (2011): Ethylene is involved in pistil fate by modulating the onset of ovule senescence and the ga-mediated fruit set in *Arabidopsis*. BMC Plant Biology, 11: 84.

Cuadrosinostroza A., Ruízlara S., Gonzalez E., Eckardt A., Willmitzer L., Peñacortés H. (2016): GC–MS metabolic profiling of Cabernet Sauvignon and Merlot cultivars during grapevine berry development and network analysis reveals a stage- and cultivar-dependent connectivity of primary metabolites. Metabolomics, 12: 39–55.

Dare A.P., Yauk Y.K., Tomes S., Mcghie T.K., Rebstock R.S., Cooney J.M. (2017): Silencing a phloretin-specific glycosyltransferase perturbs both general phenylpropanoid biosynthesis and plant development. Plant Journal, 91: 237–250.

De Vos R.C., Moco S., Lommen A., Keurentjes J.J.B., Bino R.J., Hall R.D. (2007): Untargeted large-scale plant metabolomics using liquid chromatography coupled to mass spectrometry. Nature Protocols, 2: 778–791.

Eichner J., Rosenbaum L., Wrzodek C., Haring H.U., Zell A., Lehmann R. (2014): Integrated enrichment analysis and pathway-centered visualization of metabolomics, proteomics, transcriptomics, and genomics data by using the InCroMAP software. Journal of Chromatography B, 966: 77–82.

FAO (2017): Food and Agricultura Data. Available at http://www.fao.org/faostat/zh/#data/QC.

Ferreyra M.L.F., Rius S.P., Casati P.C. (2012): Flavonoids: biosynthesis, biological functions, and biotechnological applications. Frontiers in Plant Science, 3: 222–236.

Goto K., Meyerowitz E.M. (1994): Function and regulation of the *Arabidopsis* floral homeotic gene pistillata. Genes and Development, 8: 1548–1560.

Hama E., Takumi S., Ogihara Y., Murai K. (2004): Pistillody is caused by alterations to the class-B MADS-box gene expression pattern in alloplasmic wheats. Planta, 218: 712–720.

Heischmann S., Quinn K., Cruickshank-Quinn C., Liang L.P., Reisdorph R., Reisdorph N., Patel M. (2016): Exploratory metabolomics profiling in the kainic acid rat model reveals depletion of 25-hydroxyvitamin d3 during epileptogenesis. Scientific Reports, 6: 31424.

Kaplan F., Kopka J., Sung D.Y., Zhao W., Popp M., Porat R., Guy C.L. (2007): Transcript and metabolite profiling during cold acclimation of *Arabidopsis* reveals an intricate relationship of cold-regulated gene expression with modifications in metabolite content. Plant Journal, 50: 967–981.

Lisec J., Schauer N., Kopka J., Willmitzer L., Fernie A. (2006): Gas chromatography mass spectrometry–based metabolite profiling in plants. Nature Protocols, 1: 387–396.

Liu M., Lima G.B., Mila I., Purgatto E., Peres L.E., Frasse P. (2016): Comprehensive profiling of ethylene response factor expression identifies ripening-associated ERF genes and their link to key regulators of fruit ripening in tomato (*Solanum lycopersicum*). Plant Physiology, 170: 1732–1744.

https://doi.org/10.17221/70/2019-CJGPB

Livak K., Schmittgen T.D. (2001): Analysis of relative gene expression data using real time quantitative PCR and the $22^{-\Delta\Delta ct}$ method. Methods, 25: 402–408.

Mo Y., Nagel C., Taylor L.P. (1992): Biochemical complementation of chalcone synthase mutants defines a role for flavonols in functional pollen. Proceedings of the National Academy of Sciences of the United States of America, 89: 7213–7217.

Murai K., Tsunewaki K. (1993): Photoperiod-sensitive cytoplasmic male sterility in wheat with *Aegilops crassa* cytoplasm. Euphytica, 67: 41–48.

Murai K., Takumi S., Koga H., Ogihara Y. (2002): Pistillody, homeotic transformation of stamens into pistil-like structures, caused by nuclear-cytoplasm interaction in wheat. Plant Journal, 29: 169–181.

Oberacher H., Whitley G., Berger B. (2013): Evaluation of the sensitivity of the 'Wiley registry of tandem mass spectral data, MSforID' with MS/MS data of the 'NIST/NIH/EPA mass spectral library. Journal of Mass Spectrometry, 48: 487–496.

Peer W.A., Murphy A.S. (2007): Flavonoids and auxin transport: Modulators or regulators? Trends in Plant Science, 12: 556–563.

Peng Z.S., Yang Z.J., Ouyang Z.M., Yang H. (2013): Characterization of a novel pistillody mutant in common wheat. Australian Journal of Crop Science, 7: 159–164.

Rudich J. (1969): Increase in femaleness of three cucurbits by treatment with Ethrel, an ethylene-releasing compound. Planta, 86: 69–76.

Smith C.A., Want E.J., O'Maille G., Abagyan R., Siuzdak G. (2006): XCMS: processing mass spectrometry data for metabolite profiling using nonlinear peak alignment, matching, and identification. Analytical Chemistry, 78: 779–787.

Sommer H., Beltrán J.P., Huijser P., Pape H., Lönnig W.E., Saedler H. (1990): Deficiens, a homeotic gene involved in the control of flower morphogenesis in *Antirrhinum majus*: the protein shows homology to transcription factors. Embo Journal, 9: 605–613.

Sun Q.X., Qu J.P., Yu Y., Yang Z.J., Wei S.H., Wu Y.L., Yang J., Peng Z.S. (2019): TaEPFL1, an EPIDERMAL PATTERNING FACTOR-LIKE (EPFL) secreted peptide gene, is required for stamen development in wheat. Genetica, 147: 121–130.

Takahashi H., Jaffe M. (1983): Further studies of auxin and ACC induced feminization in the cucumber plant using ethylene inhibitors. Phyton, 44: 81–86.

Tao Q., Niu H., Wang Z., Zhang W., Wang H., Wang S. (2018): Ethylene responsive factor erf110 mediates ethylene-regulated transcription of a sex determination-related orthologous gene in two cucumis species. Journal of Experimental Botany, 69: 2953–2965.

Tohge T., Nishiyama Y., Hirai M.Y., Yano M., Nakajima J., Awazuhara M. (2005): Functional genomics by integrated analysis of metabolome and transcriptome of *Arabidopsis* plants over-expressing an MYB transcription factor. Plant Journal, 42: 218–235.

Tsao T.H. (1988): Sex expression in flowering. Acta Physiologica Sinica, 14: 203–207.

Wang A., Li R., Ren L., Gao X., Zhang Y., Ma Z., Ma D., Luo Y. (2018): A comparative metabolomics study of flavonoids in sweet potato with different flesh colors (*Ipomoea batatas* (L.) Lam). Food Chemistry, 260: 124–134.

Wang K., Li H., Ecker J.R. (2002): Ethylene biosynthesis and signaling networks. Plant Cell, 14 (Suppl.): S131–S151.

Yamada K., Saraike T., Shitsukawa N., Hirabayashi C., Takumi S., Murai K. (2009): Class B and Bsister MADS-box genes are associated with ectopic ovule formation in the pistil-like stamens of alloplasmic wheat (*Triticum aestivum* L.). Plant Molecular Biology, 71: 1–14.

Yamasaki S., Fujii N., Takahashi H. (2003): Characterization of ethylene effects on sex determination in cucumber plants. Sexual Plant Reproduction, 16: 103–111.

Yang Q., Yang Z.J., Tang H.F., Yu Y., Chen Z.Y., Wei S.H., Sun Q.X., Peng Z.S. (2018): High-density genetic map construction and mapping of the homologous transformation sterility gene (hts) in wheat using GBS markers. BMC Plant Biology, 18: 301.

Yang Z.J., Peng Z.S., Yang H., Yang J., Wei S.H., Cai P. (2011): Suppression subtractive hybridization identified differentially expressed genes in pistil mutations in wheat. Plant Molecular Biology Reporter, 29: 431–439.

Yang Z.J., Peng Z.S., Wei S.H., Liao M.L., Yan Y., Jang Z.Y. (2015): Pistillody mutant reveals key insights into stamen and pistil development in wheat (*Triticum aestivum* L.). BMC Genomics, 16: 211–220.

Yang Z.J., Chen Z.Y., Peng Z.S., Yu Y., Liao M.L., Wei S.H. (2017): Development of a high-density linkage map and mapping of the three-pistil gene (*Pis1*) in wheat using GBS markers. BMC Genomics, 18: 567.

Yin T., Quinn J.A. (1995): Tests of a mechanistic model of one hormone regulating both sexes in *Cucumis sativus* (Cucurbitaceae). American Journal of Botany, 82: 1537–1546.

Yu Y., Wang T., Wu Y.C., Zhou Y.H., Jiang Y.Y., Zhang L. (2019): Effect of elicitors on the metabolites in the suspension cell culture of *Salvia miltiorrhiza* Bunge. Physiology and Molecular Biology of Plants, 25: 229–242.

Zhang Q., Xu J., Li Y., Xu P., Zhang H., Wu X. (2007): Morphological, anatomical and genetic analysis for a rice mutant with abnormal hull. Journal of Genetics and Genomics, 34: 519–526.

Zimin A.V., Puiu D., Hall R., Kingan S., Clavijo B.J., Salzberg S.L. (2017): The first near-complete assembly of the hexaploid bread wheat genome, *Triticum aestivum*. Gigascience, 6: 1–7.

Received for publication July 20, 2019
Accepted after corrections October 9, 2019
Published online November 5, 2019